Angle-resolved photoelectron spectroscopy study of the InP(100)-(2×4) surface electronic structure

W. R. A. Huff*
Research Institute for Scientific Measurements, Tohoku University, Sendai 980-77, Japan

M. Shimomura, N. Sanada, G. Kaneda, T. Takeuchi, and Y. Suzuki
Research Institute of Electronics, Shizuoka University, Hamamatsu 432, Japan

H. W. Yeom†
Research Center for Spectrochemistry, Faculty of Science, The University of Tokyo, Tokyo 113, Japan

T. Abukawa and S. Kono
Research Institute for Scientific Measurements, Tohoku University, Sendai 980-77, Japan

Y. Fukuda
Research Institute of Electronics, Shizuoka University, Hamamatsu 432, Japan
(Received 2 June 1997; revised manuscript received 12 September 1997)

The InP(100)-(2×4) surface electronic structure was studied using angle-resolved photoelectron spectroscopy together with synchrotron radiation. We identify three surface states occurring in the gaps of the projected bulk bands. The highest level state, located at binding energy $E_B = 1.0$ eV, is consistent with previous findings. The second and third states, located at $E_B = 1.8$ and 4.3 eV, have not been reported previously. All three of these surface states show no discernible dispersion as compared to the surface states on InAs(100)-(2×4) and GaAs(100)-(2×4). This result suggests that the elements of the InP(100)-(2×4) surface unit cells are more isolated from each other than they are for the InAs(100)-(2×4) or the GaAs(100)-(2×4) surface. [S0163-1829(98)04903-0]

I. INTRODUCTION

The (100) surface of group III-V semiconductors is recognized as being one of the most important surfaces to the electronics industry. However, these surfaces exhibit many different reconstructions and debates reign regarding their electronic and geometric structures.[1,2] For example, three different surface structures were recently proposed for the clean InP(100) surface.[3–5] The one area where these studies agree is that the true surface structure cannot be described by the missing row dimer (MRD) model[2] familiar to GaAs(100)-(2×4) and -(4×2). This assertion was recently supported by Pahlke *et al.*[6] The MRD model was originally proposed for the InP(100)-(2×4) surface by Hou *et al.*[7]

Most authors studying the InP(100) surface geometry have suggested a (4×2) reconstructed surface.[3,4,7] However, the orientation of the model suggested by Sung *et al.*[3] is actually a (2×4) reconstruction. MacPherson *et al.*[5] report that the surface indeed exhibits a (2×4) reconstruction. Pahlke *et al.*[6] concluded that the (2×4) surface reconstruction is obtained whether the surface is prepared by removing a passivation layer or by ion bombardment/anneal cycles. We also recently confirmed that the surface has (2×4) symmetry using x-ray photoelectron diffraction in conjunction with low-energy electron diffraction (LEED).[8] The surface Brillouin zone (SBZ) and a schematic of the ideal (1×1) surface are illustrated in Figs. 1(a) and 1(b), respectively, to clarify the [011] and the [0$\bar{1}$1] crystal axes. The irreducible (2×4) SBZ is highlighted with bold lines.

Most previous electronic structure studies of the InP(100) surface have also suggested a (4×2) surface reconstruction. None of these previous studies present a detailed band mapping of the clean InP(100) surface. Moison and Bensoussan[9] studied the surface density of states and discovered a surface state near the valence-band maximum. Hou *et al.*[7,10] and Wang[11] present detailed studies of this surface state, but only show normal emission spectra for InP(100). Lodders *et al.*[12] studied the InP(100) bulk electronic structure and map the ΓX line by changing the photon energy; however, they also present only normal-emission spectra. Weiss *et al.*[13] studied the InP(100) electronic structure, but concentrated on the CaF_2 coverage. In an inverse photoemission study, Riese, Milas, and Merz[14] show the dispersion of an empty surface state along the ×2 symmetry axis. The only theoretical study we could find was completed by Chan and Ong,[15] but they only discuss the relative stability of the (4×2), (2×2A), and (1×1) reconstructions. Finally, Mitchell *et al.*[16,17] were the first to suggest a study of the (2×4) reconstruction, but only present a detailed analysis and valence-band mapping of the sulfur-passivated surface.

We present a detailed study of the clean InP(100)-(2×4) surface electronic structure. Using angle-resolved photoelectron spectroscopy (ARPES) together with synchrotron radiation, we mapped the valence bands around the ideal (1×1) SBZ; we did not map the (2×4) SBZ because of its small size in the ×4 direction. The results are presented using a valence-band imaging technique.[18]

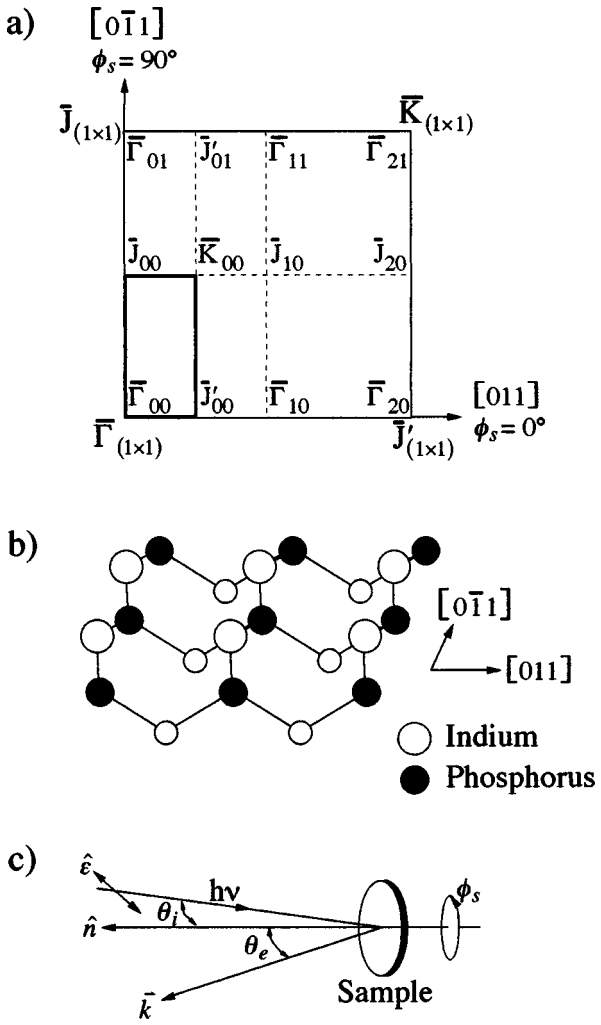

FIG. 1. (a) Schematic of the (1×1) irreducible SBZ with the (2×4) SBZ superimposed (irreducible part in bold), (b) the ideal (1×1) surface illustrating the [011] and [0$\bar{1}$1] directions, and (c) a schematic of the experimental geometry.

II. EXPERIMENT

The ARPES experiments were performed using beamline 18A at the Photon Factory, National Laboratory for High Energy Physics in Japan. This beamline is on a bending magnet and is comprised of a constant-deviation-angle grazing-incidence monochromator. The accessible photon energy range was 10–150 eV.

The sample was a *p*-type Cd-doped InP(100) wafer supplied by MaTeck (Germany); the carrier density was 2×10^{18} cm^{-3}. The epitaxial-grade surface was oriented to within 0.5°. The sample was solvent degreased and then chemically etched in H_2SO_4:H_2O_2:H_2O (3:1:1) for 10 s at 60 °C. The surface was then sulfur passivated by immersing the sample in an $(NH_4)_2S_x$ solution for 75 min at room temperature. Finally, the sample was rinsed with running deionized water before insertion into the vacuum chamber. The experimental chamber base pressure was 2×10^{-8} Pa during the data acquisition.

The sulfur was removed and the surface was cleaned by Ar^+ bombardment (500 V) followed by annealing to 300 °C for 5 min. To reduce the *P* depletion caused by the sputter/anneal cycles, the sample was sputtered at low current and as infrequently as possible to maintain a high-quality InP(100)-(2×4) surface. A commercial Vacuum Generators ADES500 hemispherical electron energy analyzer was used to collect the photoemission spectra. The angular resolution was ~±1° and the total energy resolution was ~220 meV at the two photon energies used in this study, 19.0 and 21.2 eV. No carbon or oxygen contamination was detected by x-ray photoemission spectroscopy (Mg $K\alpha$, 1253.6 eV). Other measures ensuring the sample cleanliness include the good (2×4) LEED pattern and the existence of a low binding-energy surface state in the valence-band spectra.[7]

A schematic of the experimental geometry is illustrated in Fig. 1(c). The incident photon beam was fixed at $\theta_i = -45°$; all angles are measured relative to the surface normal. The sample was aligned to the plane defined by the incident photon beam $h\nu$ and the photon polarization vector $\hat{\varepsilon}$. The surface normal $\hat{n}$ and the photoemission direction $\vec{k}$ were maintained in this plane. The dispersions were measured along the various symmetry axes by rotating the analyzer in this plane to change the photoemission angle θ_e and by adjusting the sample azimuth ϕ_s appropriately. When scanning the symmetry axes which do not include the $\bar{\Gamma}_{00}$ origin, θ_e and ϕ_s were adjusted together; θ_e and ϕ_s were calculated using the binding energy $E_B = 0.7$ eV (photoelectron kinetic energy $E_K = 18.3$ eV) as representative of the relevant values of the photoelectron wave vector's parallel component $k_\parallel$.

The raw data are a series of photoemission spectra plotted as intensity versus binding energy relative to the Fermi energy E_F. These data are reduced to a valence-band (VB) image that plots the spectral intensities with respect to the binding energy (relative to E_F) and $k_\parallel$.[18–20] The resultant VB images are a direct and compact illustration of the valence-band dispersion as well as the strength of each valence-band feature throughout the SBZ. Thus, feature identification is less arbitrary than the typical method of using filled and unfilled symbols.

III. RESULTS AND DISCUSSION

Figure 2(a) shows the raw VB spectra collected along the [011] axis from $\bar{\Gamma}_{00}$ to $\bar{\Gamma}_{20}$ at $h\nu = 19.0$ eV. Figure 2(b) shows the raw VB spectra measured along the [0$\bar{1}$1] axis from $\bar{\Gamma}_{00}$ to $\bar{\Gamma}_{01}$ at $h\nu = 19.0$ eV. Similar data (not shown) were collected along the [011] and [0$\bar{1}$1] axes at 21.2 eV to identify bulk-related features such as those which disperse with changing photon energy and surface umklapp bands. Figure 3 shows the VB images obtained from these four data sets. At a given photon energy, the bulk bands should show similar binding energies and dispersions along each symmetry axis. The bulk BZ symmetry points are indicated at the bottom of each image. Along a given symmetry axis, the surface-related features should show similar binding energies and dispersions for each photon energy. The surface BZ symmetry points are indicated at the top of each image.

As seen by Lodders *et al.*,[12] the lowest binding-energy feature associated with a bulk-band emission *B* (dashed line) shows little dispersion in this photon energy range at normal emission, $\bar{\Gamma}_{(1\times1)}$. However, at the $J_{(1\times1)}$ ($J'_{(1\times1)}$) point, *B* disperses to higher binding energy at the higher photon energy. Note that our definition of *J* and *J'* is consistent with

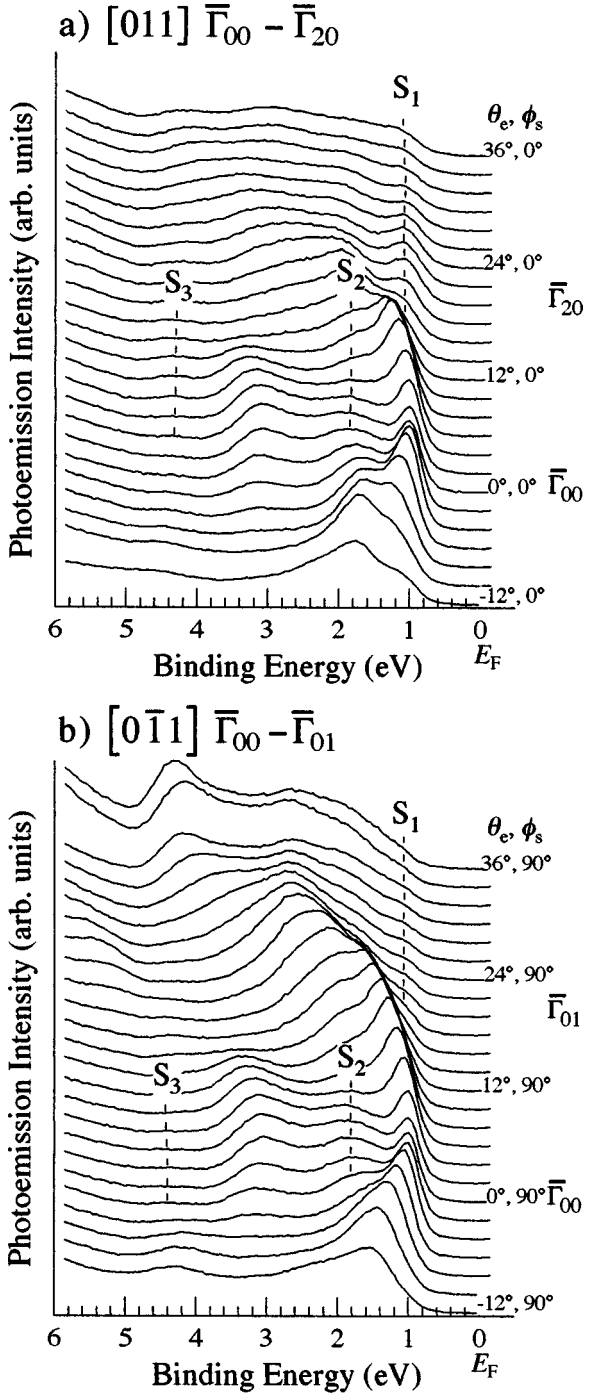

FIG. 2. Raw valence-band photoemission spectra collected at $h\nu = 19.0$ eV for the (a) [011] and (b) [0$\bar{1}$1] axes that include the $\bar{\Gamma}_{00}$ origin. $\theta_i = -45°$; ϕ_s was fixed as indicated. S_1, S_2, and S_3 indicate possible surface states.

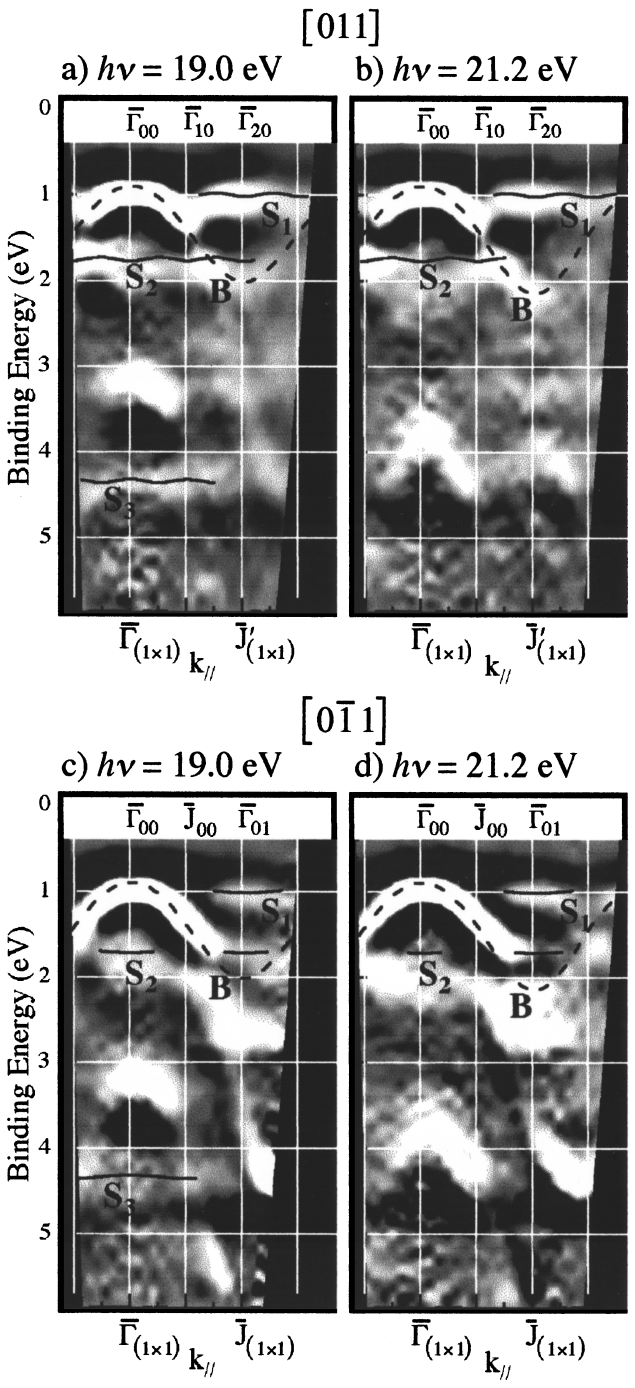

FIG. 3. Valence-band images derived from data taken at $h\nu = 19.0$ and 21.2 eV along the (a) and (b) [011] as well as the (c) and (d) [0$\bar{1}$1] symmetry axes. S_1, S_2, and S_3 indicate possible surface states.

that of Ivanov, Mazur, and Pollmann.[21] This is reversed from the definition used by Larsen and co-workers.[22–24] There are, however, two distinct bulk features at $\bar{\Gamma}_{(1\times1)}$ that disperse with changing photon energy. In Figs. 3(a) and 3(c) ($h\nu = 19.0$ eV), these are located at $E_B \approx 1.8$ eV (overlapping S_2) and 3.2 eV. In Figs. 3(b) and 3(d) ($h\nu = 21.2$ eV), these are located at $E_B \approx 2.0$ and 3.8 eV (overlapping S_3). Stietz *et al.*[25] previously discussed these two bulk features at $h\nu = 21.2$ eV.

The labels S_1, S_2, and S_3 (solid lines) indicate features that do not disperse with changing photon energy and are believed to be surface related. Because B does not disperse with changing photon energy at normal emission and because B and S_1 have similar binding energies, one must consider that S_1 could be a bulk-related surface umklapp band. If S_1 was a surface umklapp band, however, one would expect its intensity to be greater at $\bar{\Gamma}_{10}$ and lower at $\bar{\Gamma}_{20}$ in Figs. 3(a) and 3(b).[26] Due to the small SBZ size in the $\times 4$ direction, the result would be a very flat band at $E_B \sim 1$ eV across the entire SBZ. However, there is no distinguishable peak or

shoulder at the $\bar{\Gamma}_{10}$ point. Additionally, although bulk-related surface umklapp bands are repeated at the symmetry points defined by the surface reconstruction, their dispersion is directed by the bulk symmetry because they are directly related to a bulk band.[26] However, in Figs. 3(c) and 3(d), there is no indication that S_1 mimics the B dispersion.

The possibility of surface umklapp bands giving rise to S_2 is best considered by analyzing Figs. 3(c) and 3(d). If S_2 at $\bar{\Gamma}_{01}$ was a surface umklapp band relating to bulk band at Γ_{00} with a similar binding energy, then S_2 would disperse to higher binding energy at the higher photon energy as the bulk band does. Although S_2 has a relatively lower intensity at $h\nu = 21.2$ eV, its binding energy is constant with changing photon energy.

S_3 is a bit more ambiguous because it is completely obscured by a bulk band at $h\nu = 21.2$ eV. However, at $h\nu = 19.0$ eV, there appear to be no bulk bands in the vicinity of S_3.[12] Additionally, we will show that S_3 has an *increased* intensity where we expect there to be a window in the bulk-band projection. Surface umklapp bands are detected in the gaps of the bulk-band projection, but their intensity is typically lower than the principle bulk band to which they are related.[26] Thus, if S_3 was a surface umklapp band, then we would expect its intensity to be higher at $\bar{\Gamma}_{01}$ and $\bar{\Gamma}_{20}$ and lower around $\bar{\Gamma}_{21}$ [cf. Fig. 5(a)].

Figures 4(a) and 4(b) show the raw VB spectra measured along the $\bar{\Gamma}_{01}$-$\bar{\Gamma}_{11}$-$\bar{\Gamma}_{21}$ and the $\bar{\Gamma}_{20}$-$\bar{J}_{20}$-$\bar{\Gamma}_{21}$ symmetry axes [cf Fig. 1(a)] at $h\nu = 19.0$ eV. These represent the [011] and [0$\bar{1}$1] directions, respectively, for two symmetry axes that do not include the $\bar{\Gamma}_{00}$ origin. Mapping the ideal (1×1) SBZ is useful because the edge of the bulk-band projection reaches an energy-position minimum at the $\bar{K}_{(1\times1)}$ point.[21,23] This in turn makes S_1 and S_2 easier to identify. Also, a window in the bulk-band projection directly below this minimum allows the intensity of S_3 to be enhanced in these spectra.

Figure 5(a) is the valence-band image plotting binding energy (eV) versus $k_\parallel$ (Å^{-1}) constructed from the four data sets presented in Figs. 2 and 4. S_1, S_2, and S_3 are highlighted with solid lines. The edge of the bulk-band projection B is indicated with a dashed line. We obtained the $\bar{\Gamma}_{(1\times1)}$ point and the $\bar{K}_{(1\times1)}$ point binding energies by relating bulk-band structure calculations to the bulk Brillouin zone geometry.[15,27–29] In the absence of a calculated bulk-band projection for InP(100), we used the GaAs(100) calculated bulk-band projection to estimate the shape of B.[21,23] After additionally considering the available bulk projection calculations for InSb(100) (Ref. 30) and InAs(100),[31] we expect a window in the projected bulk bands to be centered below the $\bar{K}_{(1\times1)}$ point.

Figure 5(a) clearly illustrates that S_1 and S_2 occur in the bulk band gap. The intensity of S_3 is enhanced in the region where we expect the window at the $\bar{K}_{(1\times1)}$ point. A conservative assignment of this window is drawn in Fig. 5(b) by noting the region where S_3 has enhanced intensity; we expect the true window to encompass more than just the area indicated.

The surface state S_1 has been reported previously.[7,9–11] In agreement with these earlier studies, the valence-band maximum (VBM) is ~0.9 eV below the Fermi edge and S_1 is ~0.1 eV below the VBM. Neither S_2, $E_B = 1.8$ eV, nor S_3, $E_B = 4.3$ eV, have been reported previously. S_2 and S_3 are easily detected in the gaps of the bulk-band projection and they are not surface umklapp bands, as already discussed. Thus, S_2 and S_3 are surface states. Similar arguments have been applied to the InSb(100) (Ref. 30) and InAs(100) (Ref. 31) surfaces.

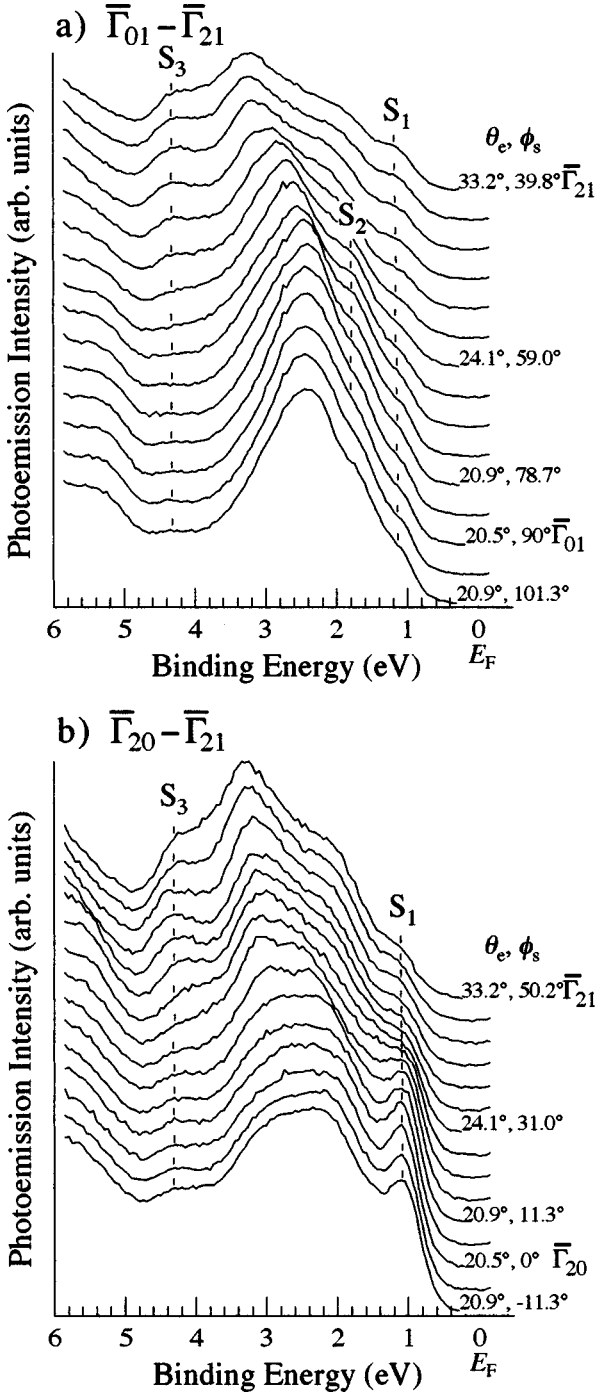

FIG. 4. Raw valence-band photoemission spectra collected at $h\nu = 19.0$ eV for (a) [011] and (b) [0$\bar{1}$1] axes that do not include the $\bar{\Gamma}_{00}$ origin. $\theta_i = -45°$; θ_e and ϕ_s were varied together to maintain $k_\parallel$ for $E_B = 0.7$ eV constant along the (a) $\bar{J}_{(1\times1)}$–$\bar{K}_{(1\times1)}$ and (b) $\bar{J}'_{(1\times1)}$–$\bar{K}_{(1\times1)}$ axes. S_1, S_2, and S_3 indicate possible surface states.

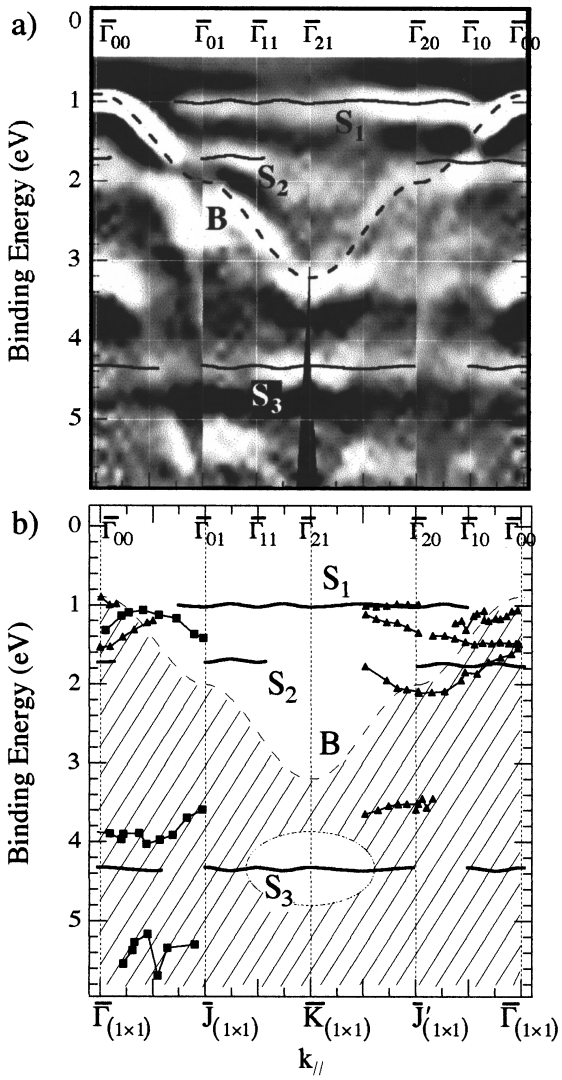

FIG. 5. (a) Valence-band image for InP(100)-(2×4) data presented in Figs. 2 and 3. The (1×1) SBZ symmetry axes are indicated at the bottom of the figure and those for the (2×4) SBZ at the top. The edge of the bulk-band projection *B* is indicated with a dashed line while solid lines indicate S_1, S_2, and S_3. (b) Schematic of the VB image in (a). The hashed part illustrates the bulk-band projection. The squares represent InAs(100)-(2×4) surface states from Ref. 31; the triangles represent GaAs(100)-(2×4) surface states from Refs. 23 and 24.

Figure 5(b) superimposes our InP(100)-(2×4) data with the InAs(100)-(2×4) data from Håkansson *et al.*[31] (squares) and with the GaAs(100)-(2×4) data from Larsen and co-workers[23,24] (triangles). The InAs and GaAs geometric surface structures are similar to each other. Both are comprised of an extended array of As dimers and their respective scanning tunneling microscopy (STM) images are nearly identical.[32,33] Although the InAs and GaAs surface states shown in Fig. 5(b) have different binding energies, states on both surfaces show dispersion resulting from the delocalized nature of their geometric structures.

In contrast, the InP(100) STM images differ from the InAs and GaAs STM images.[4,5] The surface electronic structure comparison in Fig. 5(b) also shows differences. Unlike the InAs and GaAs surface states, the InP surface states show no discernible dispersion. This result suggests that the elements of the InP surface unit cells are more localized than those of the InAs or GaAs surface unit cells. Note that Pahlke *et al.*[6] also suggested that the detailed InP(100)-(2×4) geometric structure differs from the accepted GaAs(100)-(2×4) structure. Structure-dependent valence-band calculations should be completed and compared to the experimental valence-band data presented here to provide more information about the local atomic geometry. Such calculation results will also help to identify the origins of the InP(100)-(2×4) surface states.

IV. CONCLUSION

We studied the InP(100)-(2×4) surface electronic structure using angle-resolved photoelectron spectroscopy together with synchrotron radiation. We identify three surface states occurring in the gaps of the projected bulk bands. The highest level state, $E_B = 1.0$ eV, is consistent with previous findings. The second state, $E_B = 1.8$ eV, and the third state, $E_B = 4.3$ eV, have not been reported previously.

In contrast to the surface states reported for InAs(100)-(2×4) and GaAs(100)-(2×4), the InP(100)-(2×4) surface states exhibit no discernible dispersion. This result indicates that the elements of the surface unit cells are more isolated from each other on the InP surface than they are on the InAs or GaAs surfaces. These InP valence band data alone are not sufficient to yield information regarding the local atomic geometry or the origins of the three surface states. Structure-dependent valence-band calculations are required to learn more about the physics behind the three InP(100)-(2×4) surface states.

ACKNOWLEDGMENTS

We gratefully acknowledge Professor A. Kakizaki, Dr. A. Kimura, and A. Harasawa from the Institute for Solid State Physics in Tokyo for their generous support and allotment of beamtime. This work was performed under the Photon Factory proposal No. 96G277.

*Present address: KLA-Tencor, Milpitas, CA 95035.
†Author to whom correspondence should be addressed.

[1] G. V. Hansson and R. I. G. Uhrberg, Surf. Sci. Rep. **9**, 197 (1988).
[2] C. B. Duke, Chem. Rev. **96**, 1237 (1996).
[3] M. M. Sung, C. Kim, H. Bu, D. S. Karpuzov, and J. W. Rabalais, Surf. Sci. **322**, 116 (1995).
[4] M. Shimomura, N. Sanada, Y. Fukuda, and P. J. Møller, Surf. Sci. Lett. **359**, L451 (1996).
[5] C. D. MacPherson, R. A. Wolkow, C. E. J. Mitchell, and A. B. McLean, Phys. Rev. Lett. **77**, 691 (1996).
[6] D. Pahlke, J. Kinsky, Ch. Schultz, M. Pristovsek, M. Zorn, N. Esser, and W. Richter, Phys. Rev. B **56**, R1661 (1997).
[7] X.-Y. Hou, G.-S. Dong, X.-M. Ding, and X. Wang, J. Phys. C **20**, L121 (1987).
[8] M. Shimomura, N. Sanada, G. Kaneda, T. Takeuchi, Y. Suzuki, Y. Fukuda, W. R. A. Huff, T. Abukawa, S. Kono, H. W. Yeom, and A. Kakizaki, Surf. Sci. Lett. (to be published).

[9] J. M. Moison and M. Bensoussan, Surf. Sci. **168**, 68 (1986).
[10] X.-Y. Hou, G.-S. Dong, X.-M. Ding, and X. Wang, Surf. Sci. **183**, 123 (1987).
[11] X. Wang, Appl. Surf. Sci. **33/34**, 88 (1988).
[12] F. Lodders, J. Westhof, J. A. Schaefer, H. Höpfinger, A. Goldmann, and S. Witzel, Z. Phys. B **83**, 263 (1991).
[13] W. Weiss, R. Hornstein, D. Schmeisser, and W. Göpel, J. Vac. Sci. Technol. B **8**, 715 (1990).
[14] S. Riese, E. Milas, and H. Merz, Surf. Sci. **269/270**, 833 (1992).
[15] B. C. Chan and C. K. Ong, J. Phys. Chem. Solids **52**, 699 (1991).
[16] C. E. J. Mitchell, I. G. Hill, A. B. McLean, and Z. H. Lu, Prog. Surf. Sci. **50**, 325 (1995).
[17] C. E. J. Mitchell, I. G. Hill, A. B. McLean, and Z. H. Lu, Appl. Surf. Sci. **104/105**, 434 (1996).
[18] T. Abukawa, M. Sasaki, F. Hisamatsu, T. Goto, T. Kinoshita, A. Kakizaki, and S. Kono, Surf. Sci. **325**, 33 (1995).
[19] H. W. Yeom, T. Abukawa, Y. Takakuwa, M. Nakamura, M. Kimura, A. Kakizaki, and S. Kono, Surf. Sci. Lett. **321**, L177 (1994).
[20] H. W. Yeom, T. Abukawa, Y. Takakuwa, Y. Mori, T. Shimatani, A. Kakizaki, and S. Kono, Phys. Rev. B **53**, 1948 (1996).
[21] I. Ivanov, A. Mazur, and J. Pollmann, Surf. Sci. **92**, 365 (1980).
[22] P. K. Larsen, J. H. Neave and B. A. Joyce, J. Phys. C **14**, 167 (1981).
[23] P. K. Larsen, J. F. van der Veen, A. Mazur, J. Pollmann, J. H. Neave, and B. A. Joyce, Phys. Rev. B **26**, 3222 (1982).
[24] P. K. Larsen and J. F. van der Veen, J. Phys. C **15**, L431 (1982).
[25] F. Stietz, Th. Allinger, V. Polyakov, J. Woll, A. Goldmann, W. Erfurth, G. J. Lapeyre, and J. A. Schaefer, Appl. Surf. Sci. **104/105**, 169 (1996).
[26] G. Lévêque, M. Banouni, C. Jouanin, D. Bertho, and J. Bonnet, J. Vac. Sci. Technol. A **11**, 529 (1993).
[27] L. W. James, J. P. Van Dyke, F. Herman, and D. M. Chang, Phys. Rev. B **1**, 3998 (1970).
[28] J. R. Chelikowsky and M. L. Cohen, Phys. Rev. B **14**, 556 (1976).
[29] E. W. Plummer and W. Eberhardt, Adv. Chem. Phys. **49**, 533 (1982).
[30] L. O. Olsson, Y. O. Khazmi, J. Kanski, L. Ilver, P. O. Nilsson, M. C. Håkansson, and U. O. Karlsson, Surf. Sci. **331–333**, 1176 (1995).
[31] M. C. Håkansson, L. S. O. Johansson, C. B. M. Andersson, U. O. Karlsson, L. Ö. Olsson, J. Kanski, L. Ilver, and P. O. Nilsson, Surf. Sci. **374**, 73 (1997).
[32] A. R. Avery, D. M. Holmes, J. Sudijono, T. S. Jones, and B. A. Joycc, Surf. Sci. **323**, 91 (1995).
[33] H. Yamaguchi and Y. Horikoshi, Phys. Rev. B **51**, 9836 (1995).